JOURNAL OF MATERIALS SCIENCE **38** (2003) 1383–1389

Properties of squeeze cast Mg-10Al-Mn alloy and its alumina short fibre composites

S. JAYALAKSHMI, S. V. KAILAS, S. SESHAN
Department of Mechanical Engineering, Indian Institute of Science, Bangalore 560 012, India
E-mail: office@mecheng.iisc.ernet.in

Magnesium alloys are very suitable for applications that require materials with high strength-to-weight ratio. However, the use of magnesium alloys is limited due to their low elevated temperature properties. Magnesium matrix composites are the possible alternatives. The present work involved the production and subsequent property evaluation of AM100 magnesium alloy and its alumina short fibre reinforced composites. Studies on microstructure, hardness, density, stiffness, tensile properties, impact strength, wear resistance and corrosion resistance were carried out. Results indicate the significant improvement in the properties achieved by making composites. The findings also highlight the dominant roles of the base alloy matrix and the fibre volume fraction in determining the above properties.

1. Introduction

Magnesium, with a low density of 1.7 gm/cm^3 is highly suitable for applications where weight reduction is critical [1, 2]. The other advantages include satisfactory room temperature properties, damping capacity and electrical & thermal conductivities [2]. There is a growing demand for magnesium and its alloys in aerospace, automobile and transport industries as structural materials. However, their applications are limited due to the lowering of strength when exposed to elevated temperatures [3]. It has been widely reported that metal matrix composites (MMCs) are suitable alternatives for improving properties such as strength, stiffness, hardness, wear resistance and creep resistance. Such improvements have been observed earlier in MMCs based on aluminium, copper, zinc and titanium alloys [4–7]. Among the processing methods employed for producing MMCs, the squeeze casting route appears to be the most economical. The MMCs so produced show excellent grain refinement and negligible porosity [4, 8]. This process, called the squeeze infiltration technique, is widely used for the production of short fibre reinforced composites [9]. Reinforcing magnesium base alloys with ceramic additions is likely to improve some of the properties. However, literature available on magnesium composites is rather meager when compared to data on MMCs based on other non-ferrous alloys.

In the work reported here, AM100 magnesium alloy was used as the base matrix with alumina short fibres as reinforcements. As magnesium metal is difficult to handle in the molten state [10], the process parameters employed during melting and casting were optimized systematically to achieve sound castings, and subsequently MMCs were produced. The base alloy and the composite castings were characterized for microstructure, mechanical properties, wear resistance and corrosion resistance. The results obtained were studied for the influence of the fibre, matrix and the interface on the above properties.

2. Experimental details

Test castings of the alloy selected, viz., AM100 (Mg-9.3 to 10.7Al-0.13Mn), were produced using the squeeze casting technique. Magnesium was melted using the flux-less process [10] in a reducing atmosphere to prevent oxidation of the molten metal. Alumina (saffil) short fibre preforms of three different volume fractions (15, 20 and 25% respectively) were used as reinforcements for subsequent production of MMCs. The preforms were 70 mm in diameter and 35 mm in height. The squeeze pressure was maintained at 40 MPa and the preform temperature was 850°C for all fibre volume fractions. The castings produced were optimized for their aging response in order to achieve peak hardness. Density and modulus of elasticity were determined using the specific gravity method and elastosonic non-destructive testing method respectively. For the evaluation of tensile properties at different temperatures, tensile tests were conducted at a controlled strain rate of 0.001 s^{-1} in a Monsanto Tensometer fitted with a high temperature furnace. Impact tests were performed using a Charpy instrumented impact-testing machine. Dry sliding wear tests were conducted on a pin-on-disc facility with (a) EN24 steel disc and (b) SiC abrasive disc as the counterface disc materials. Corrosion tests were carried out in a salt spray atmosphere [11]. Optical and scanning electron microscopes were used to analyze the surfaces of the tested specimens.

3. Results and discussion

3.1. Microstructure and aging response

The microstructure of the peak hardened AM100 unreinforced alloy (Fig. 1a) shows that the eutectic (α-Mg matrix + β-$Mg_{17}Al_{12}$) is distributed along the grain boundaries. On aging, the hard and brittle β-$Mg_{17}Al_{12}$ precipitates form within the eutectic, thus producing a network along the grain boundaries [9, 12, 13]. In the composites, the sufficiently higher temperature of the preform (850°C) that is higher than that of the molten metal (~790°C), enabled complete infiltration of the molten metal into the preform and hence prevented premature solidification of the metal. The microstructure of the AM100 composite of 20% V_f (Fig. 1b) shows uniform distribution of fibres, thereby indicating the effectiveness of the squeeze infiltration process. The short fibres are distributed in a planar, random orientation due to the method of production of the preform [12]. The peak hardness and peak aging time of the unreinforced alloy and its composites are shown in Figs 2a and b. It can be observed that the hardness of the composites is twice that of the unreinforced alloy, and the hardness increases with increase in fibre volume fraction (Fig. 2a). It is also observed that with increasing volume fraction of fibres, a reduction in the peak aging time occurs (Fig. 2b). This is because, the addition of fibres provides heterogeneous nucleation sites at fibre/matrix interface for precipitation to occur, thereby accelerating the aging kinetics, leading to a large increase in hardness and a decrease in aging time [14–16].

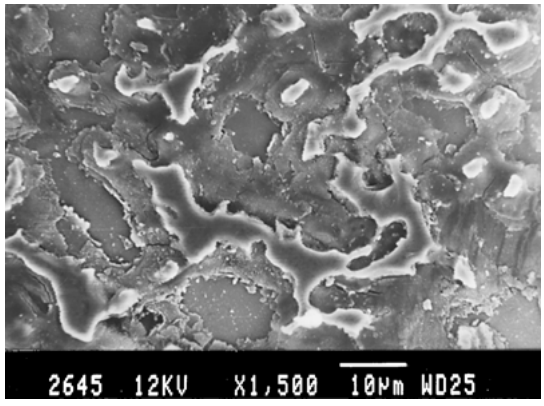

(a)

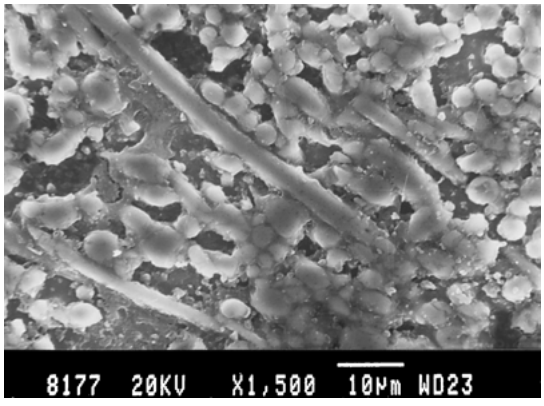

(b)

Figure 1 Microstructures of (a) AM100 alloy (b) AM100 + 20% V_f composite.

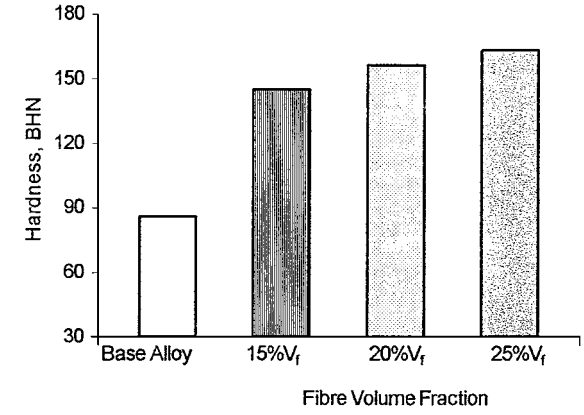

(a)

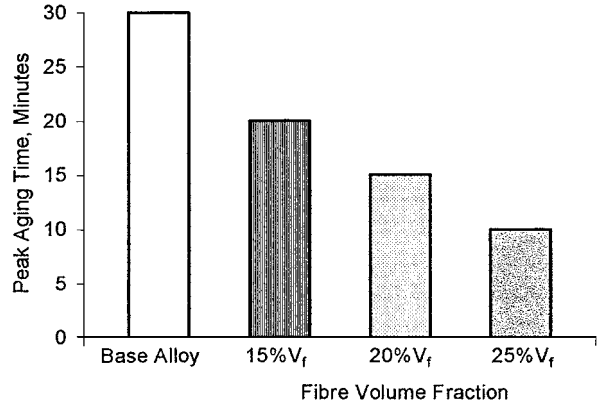

(b)

Figure 2 (a) Peak hardness of AM100 alloy and its saffil alumina fibre composites. (b) Peak aging times for AM100 alloy and its saffil alumina fibre composites.

3.2. Density and modulus of elasticity

The density values of the unreinforced alloy and its composites are shown in Table I. The increase in density of the composites is due to the higher density of the alumina fibre reinforcement (3.3 g/cm^3) as against

TABLE I Density values of AM100 alloy and its alumina short fibre composites

Fibre volume	Density (gm/cm^3)
Base alloy	1.79
15%	2.07
20%	2.17
25%	2.29

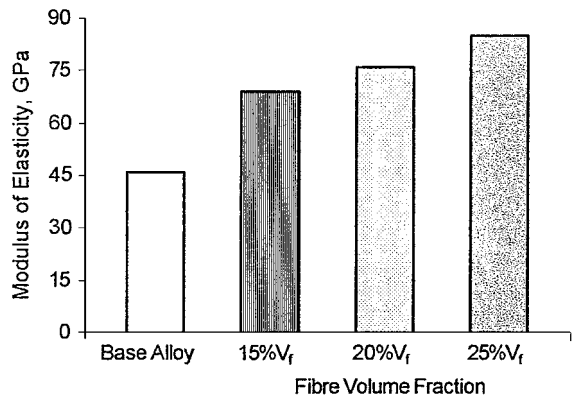

Figure 3 Variation of elastic modulus of AM100 alloy and its saffil alumina fibre composites.

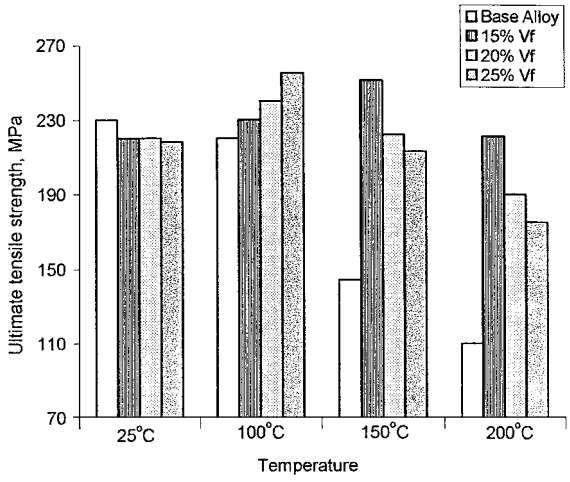

Figure 4 Ultimate tensile strength of AM100 alloy and its composites at different temperatures.

the lighter base alloy (1.8 g/cm^3). Fig. 3 indicates that the elastic modulus increases with increase in fibre volume fraction. It may be obviously observed that the modulus of the composites, particularly at the highest volume fraction of 25%, is almost twice that of the unreinforced alloy. This large improvement in the elastic modulus is attributed to the high inherent stiffness of the ceramic reinforcement.

3.3. Tensile properties

Fig. 4 shows the variation of ultimate tensile strength of the unreinforced alloy and its composites at different test temperatures. At room temperature, the base alloy possesses higher strength than the composites. Fractographic study of the base alloy shows that at room temperature the alloy fails by intergranular brittle failure (Fig. 5a). This is due to the presence of hard and

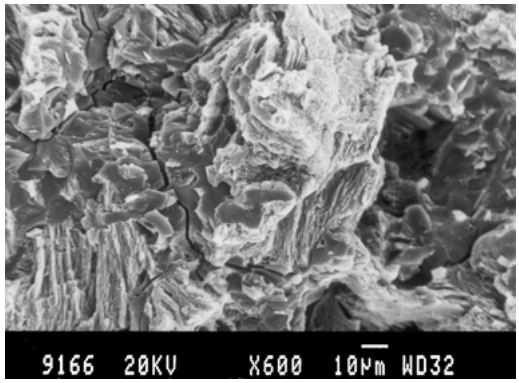

(a)

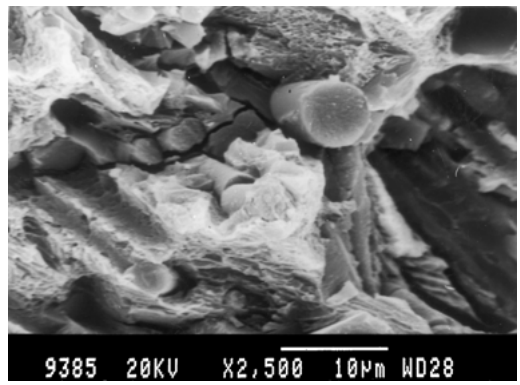

(b)

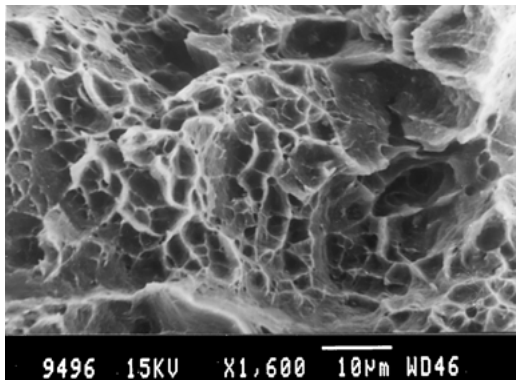

(c)

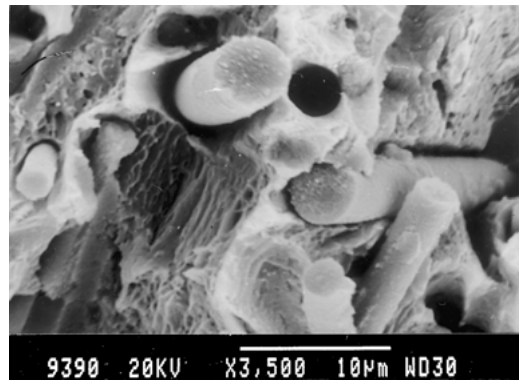

(d)

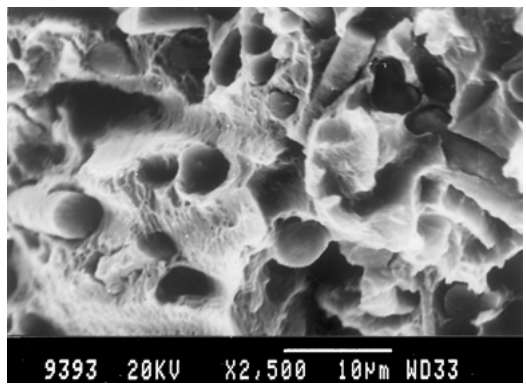

(e)

Figure 5 Fractographic evidences showing (a) intergranular failure of AM100 alloy at room temperature, (b) large matrix cracking of AM100 composite at room temperature, (c) ductile failure of unreinforced alloy at 150°C, (d) fibre participation in load transfer at 150°C (20% V_f) and (e) fibre pull-outs and fibre deformation at 200°C (20% V_f).

brittle $Mg_{17}Al_{12}$ along the grain boundaries. In the composites, at room temperature the thermal mismatch between the fibre and the matrix leads to thermal residual tensile stresses in the matrix [17, 18]. These stresses together with the applied tensile stress are high enough to cause easy failure of the composite. In addition, as the brittle $Mg_{17}Al_{12}$ precipitates form at the fibre/matrix interface, the high stresses would result in cracking of the brittle matrix. Similar observation was made earlier by Metcalfe [19] on studies involving the effect of residual tensile stresses on metal matrix composites. The fracture surface of AM100 composite (Fig. 5b) thus shows large matrix cracking. Such matrix cracking prevents efficient load transfer from the matrix to the fibre and hence results in lower strength. This further indicates the dominance of the brittle matrix in controlling the room temperature behaviour.

With increase in test temperature, the unreinforced base alloy shows a monotonic decrease in strength, whereas the composites do not exhibit such decrease. The composites retain their strength at higher temperatures (upto 200°C), indicating enhanced thermal stability compared to that of the unreinforced alloy. This stability is due to the relaxation of the residual stresses and softening of the matrix at higher temperatures, resulting in efficient load transfer from the matrix to the fibres [17]. Fig. 5c shows ductile failure of the base alloy at 150°C and Fig. 5d (composite at 150°C) shows increased ductility of the matrix along with few fibre pull-outs and fibre debonding, indicating their participation with increased temperature. However, at 150°C a reversal in trend is observed, that is, MMC with the highest volume fraction exhibits the lowest strength. This may be attributed to the rapid overaging of higher volume fraction composites (as seen from its lowest peak hardening time, Fig. 2b). This results in weak interfacial bonding and easy fibre pull-outs (Fig. 5e), leading to reduced strength. Such an influence of overaging on the strength has been observed earlier in aluminium composites [17, 20]. Fig. 6 shows the elongation values of the composites that are much lower when compared to the unreinforced alloy. This is due to the hard and brittle nature of the ceramic fibres.

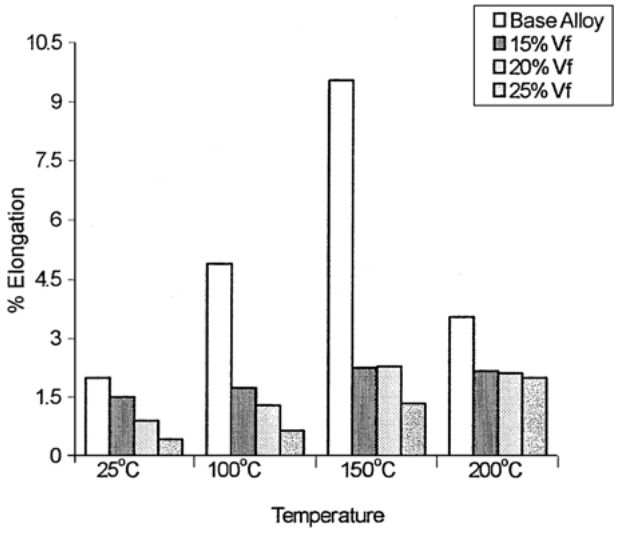

Figure 6 % Elongation of AM100 alloy and its composites at different temperatures.

3.4. Impact strength

Fig. 7 shows the total impact energy of AM100 alloy and its composites as a function of fibre volume fraction. The impact energy required for fracture reduces rapidly with addition of ceramic reinforcements, which

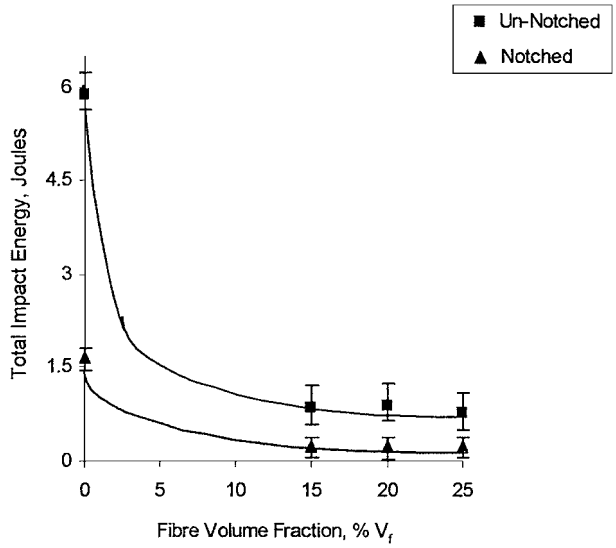

Figure 7 Variation of total impact energy of AM100 alloy and its composites.

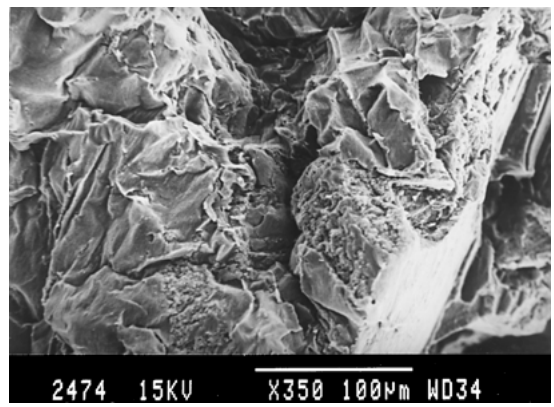

(a)

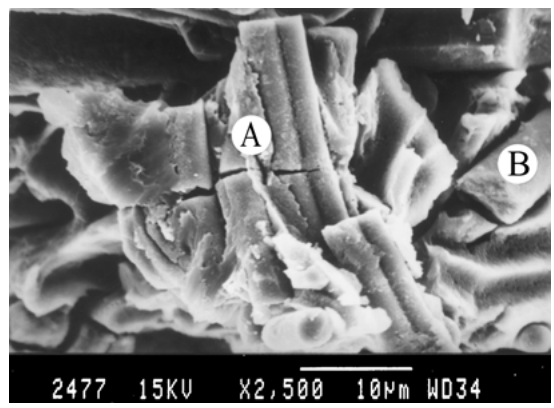

(b)

Figure 8 Fractograph showing (a) AM100 alloy-intergranular failure and (b) AM100 composite—crack propagation through fibres (A) and fibre breakage & fibre chopping (B).

is due to their inherently brittle nature. For both the alloy and its composites, the presence of notch increases the stress concentration at the tip of the notch leading to a further reduction in the impact energy [7, 12, 21]. Fractographic evidence of the unreinforced alloy shows dominant intergranular failure (Fig. 8a). This is due to the reason that the base alloy is inherently brittle due to the presence of brittle $Mg_{17}Al_{12}$ precipitates along the grain boundaries [12, 13]. Hence, addition of fibres would lead to the formation of these brittle precipitates at the fibre/matrix interface resulting in easy propagation of cracks under impact loading. This can be observed from Fig. 8b, which shows a crack propagating through fibres. Such low resistance to crack propagation results in very low absorption energy [12, 22] and eventually causes intense fibre breakage and fibre chopping (Fig. 8b).

3.5. Wear resistance and friction

The wear rate of AM100 alloy and its composites (slid against two counterface disc materials) is shown in Fig. 9a. Against both the counterfaces, the composites exhibit higher wear resistance than the base alloy due to the presence of hard ceramic reinforcement. For the alloy as well as its composites, wear rate is higher against SiC abrasive disc than against the EN24 counterface disc. This is due to the higher hardness and higher roughness of the SiC abrasive media compared to the relatively smoother EN24 counterface. In EN24 counterface, the composites exhibit decreased wear rate with increasing volume fraction. On the other hand, against SiC counterface, there is an increase in wear rate at the highest volume fraction of 25%. This increase may be due to the trapping of wear debris containing large amount of hard ceramic fibres in-between the abrasive grits of the SiC counterface. These trapped debris act as third-body and contribute to the increase in the wear rate of the composite. Fig. 9b shows the variation of co-efficient of friction of the unreinforced alloy and the composites. It is interesting to note that the coefficient of friction increases with increasing fibre volume fraction against both the counterfaces. This is probably due to the counter abrasion of the disc by the hard ceramic fibres. Fig. 10a and b shows the representative worn surface analysis of the alloy and composite. The base alloy undergoes adhesion, whereas material removal in the composites occurs by delamination. It has been reported earlier [23] that materials such as pure aluminium, AZ91 magnesium alloy and their saffil fibre reinforced composites also exhibit similar material removal processes.

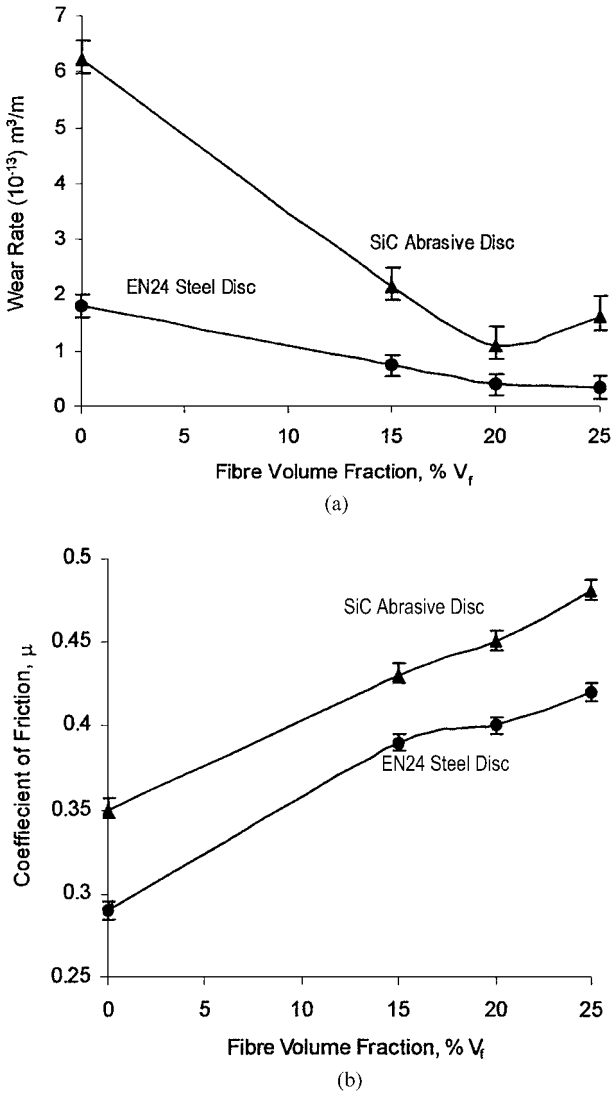

Figure 9 (a) Wear rate of unreinforced AM100 alloy and its composites sliding against two different counterfaces. (b) Coefficient of friction of unreinforced AM100 alloy and its composites sliding against two different counterfaces.

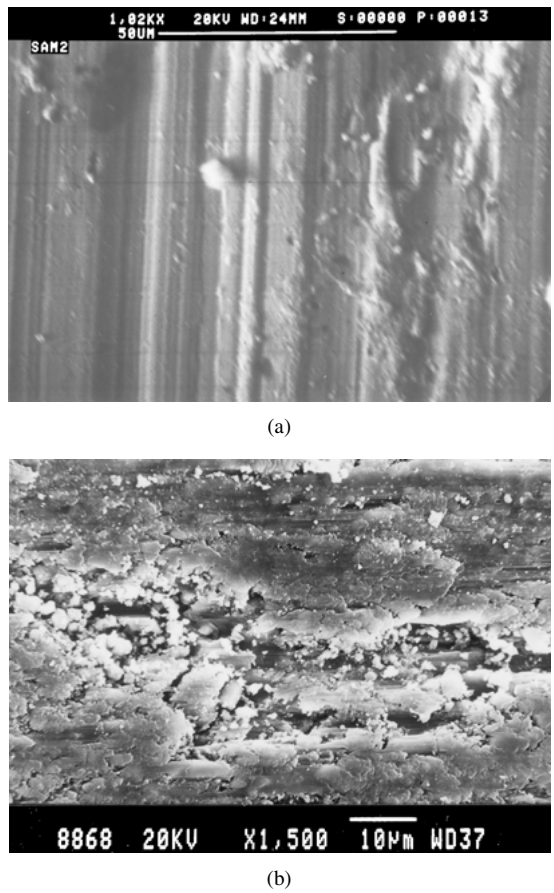

Figure 10 Worn surface of (a) AM100 alloy showing micro-ploughing and adhesion (EN24 counterface) and (b) AM100 composite showing delamination with debris trapped in the delaminated pit (SiC counterface).

4. Corrosion resistance

Fig. 11 shows the corrosion resistance of alloy AM100 and its composites as a function of exposure time. The base alloy exhibits higher corrosion resistance than its composites. In the composites, the corrosion rate initially increases with increase in fibre volume fraction. This increase in corrosion rate of the composites is due to the increase in the number of cathodic sites. In the Mg-Al-Mn system, the precipitates $Mg_{17}Al_{12}$ act as cathodic sites during corrosion [24]. Any addition of fibres increases the formation of these precipitates along the fibre matrix/interface, leading to an increase in the number of cathodic sites. Initially, this leads to a rapid dissolution of the anodic magnesium matrix. However, with further increase in exposure time, the corrosion rate decreases. This is because, the initial rapid corrosion causes deposition of corroded products on the surface and thereby prevents the exposure of fresh metal surface to the salt fog environment.

Fig. 12 shows the corroded surface of AM100 alloy that indicates uniform corrosion. The occurrence of this uniform corrosion can be explained on the basis of the 'particle undermining model' proposed by Song *et al*. [25], (Fig. 13a). The highly cathodic precipitates and the eutectic, that are present on the grain boundaries and along the fibre/matrix interface (Fig. 1a), cause initiation of corrosion within the grains (anodic Mg-matrix). This proceeds throughout the anodic matrix, finally undermining these cathodic sites (precipitates). Optical microscopic evidences confirm this mechanism (Fig. 13b and c).

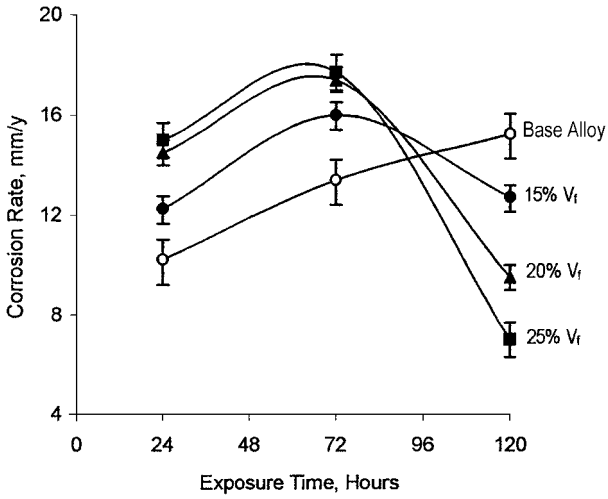

Figure 11 Variation of corrosion rate of AM100 alloy and its composites on exposure to salt fog environment.

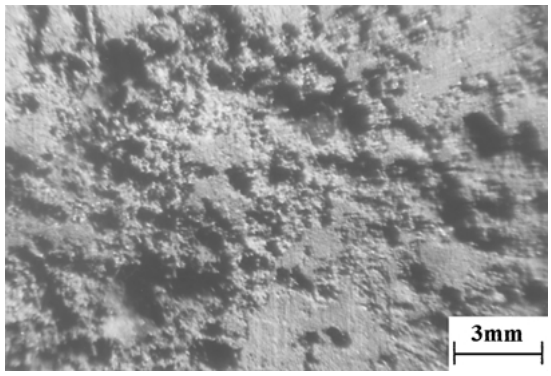

Figure 12 Low magnification micrograph showing uniform corrosion in unreinforced AM100 alloy.

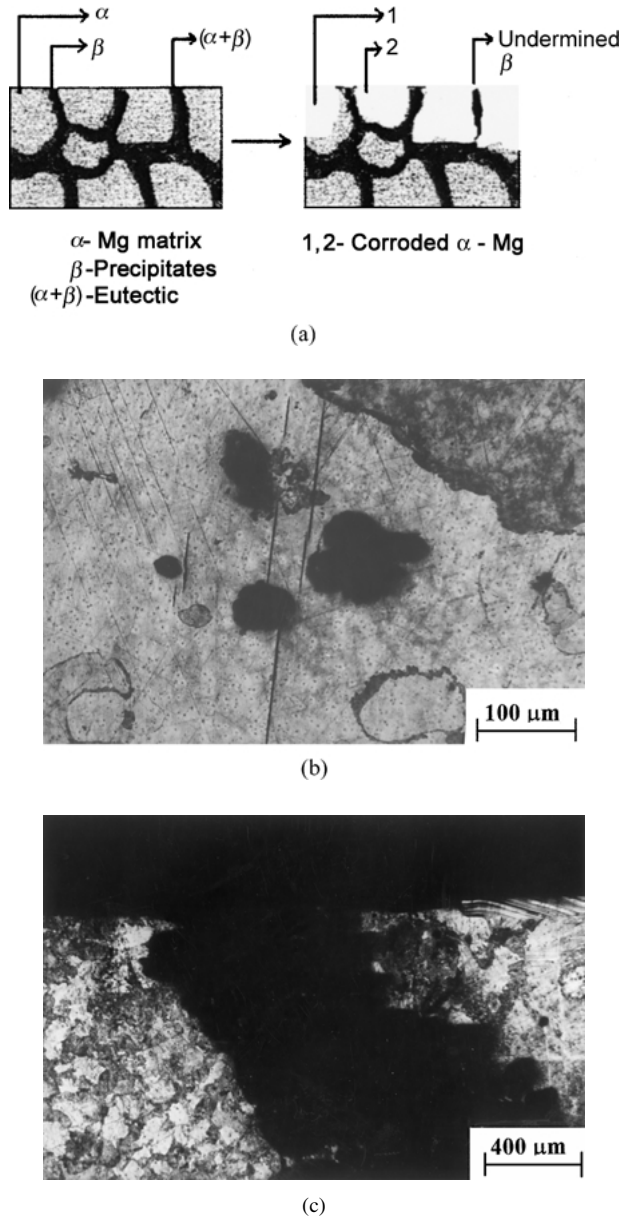

Figure 13 (a) Schematic showing the particle undermining model [25]. (b) & (c) Optical microscopic evidences showing the particle undermining model on the corroded surface of AM100 alloy.

5. Conclusions

(1) Addition of alumina fibres to AM100 alloy significantly alters the precipitation process, resulting in the acceleration of precipitation kinetics during aging.

(2) Although the composites do not show improvement in strength at room temperature, they exhibit improved elevated temperature properties and higher thermal stability when compared to the unreinforced alloy. The difference in behaviour at room and elevated temperatures is attributed to the base matrix microstructure and the fibre volume fraction.

(3) The low impact strength and corrosion resistance of composites appear inevitable. The presence of brittle ceramic fibres and the uniform distribution of precipitates along the grain boundaries and interfaces contribute to this.

(4) Although the composites exhibit higher wear resistance than the unreinforced alloy, the fibre volume fraction appears to have a distinct influence on the wear behaviour of the composites.

References

1. N. C. SPARE, Proc. of London Conference, Nov 1986, p. 101.
2. A. LUO and M. O. PERQULERYUZ, *J. Mater. Sci.* **29** (1994) 5259.
3. E. F. EMLEY, in "Principles of Magnesium Technology" (Pergamon Press, London, 1966).
4. A. A. DAS and S. CHATTERJEE, *The Metall. & Mat. Tech.* (1981) 137.
5. P. K. ROHATGI, R. ASTHANA and S. DAS, *Intl. Metals Rev.* **31**(3) (1986) 115.
6. T. W. CHOU, A. KELLY and A. OKURA, *Composites* **16** (1985) 187.
7. M. J. DELLIS, J. P. KEUSTERMANS and F. DELANNAY, *Mat. Sci. & Eng.* A **135** (1991) 253.
8. G. A. CHADWICK, *ibid.* A **135** (1991) 23.
9. H. HU, *J. Mater. Sci.* **33** (1998) 1579.
10. "Recommended Practices for Sand Casting of Aluminium & Magnesium Alloys," 2nd ed. (American Foundryman Society, Des Plaines, IL, 1965).
11. "Standard Practice for Operating Standard Salt Spray (fog) Apparatus," ASTM B 117, 1994.
12. K. PURAZRANG, K. U. KAINER and B. L. MORDIKE, *Composites* **22**(6) (1991) 456.
13. S. JAYALAKSHMI, SATISH V. KAILAS and S. SESHAN, *Composites* A, in press.
14. R. J. ARSENAULT and R. M. FISHCER, *Scripta Metall.* **17** (1983) 67.
15. S. SURESH, T. CHRISTMAN and Y. SUGIMURA, *ibid.* **23** (1989) 1599.
16. T. CHRISTMAN and S. SURESH, *Acta Metall.* **36** (1988) 1691.
17. S. J. HARRIS, *Mat. Sci. & Tech.* **4** (1988) 231.
18. C. M. FRIEND, *Scripta Metall.* **23** (1989) 33.
19. A. G. METCALFE, in "Interfaces in Metal Matrix Composites," Vol. 1, edited by. L. J. Broutman and Richard H. Brook (Academic Press, New York, 1974), ch. 1.
20. T. LIM, Y. H. KIM, C. S. LEE and K. S. HAN, *J. Comp. Mat.* **26**(7) (1992) 1062.
21. GEORGE E. DIETER, in "Mechanical Metallurgy," Metric Edition, Material Science and Metallurgy (McGraw Hill, 1988).
22. T. LIM, S. Y. LEE and K. S. HAN, in *Proc. Amer. Soc. Comp.* Ohio, June 1989, p. 84.
23. I. M. HUTCHINGS, *Mat. Sci. & Tech.* **10** (1994) 513.
24. O. LUNDER, J. E. LEIN, T. Kr. AUNE and K. NISANCIOGLU, *Corrosion* **45**(9) (1989) 741.
25. G. L. SONG and A. ATRENS, *Adv. Eng. Mat.* **1**(1) (1999) 11.

Received 30 July
and accepted 20 November 2002